Accounting for Triplet and Saturation Effects in FCS Measurements

Lloyd M. Davis and Guoqing Shen,

Center for Laser Applications, University of Tennessee Space Institute, Tullahoma, TN 37388

Abstract:
Fluorescence correlation spectroscopy (FCS) is an increasingly important tool for determining low concentrations and dynamics of molecules in solution. Oftentimes triplet transitions give rise to fast blinking effects, which are accounted for by including an exponential term in the fitting of the autocorrelation function (ACF). In such cases, concomitant saturation effects also modify the amplitude and shape of the remaining parts of the ACF. We review studies of triplet and saturation effects in FCS and present a simple procedure to obtain more accurate results of particle concentrations and diffusional dynamics in experiments where triplet kinetics are evident, or where moderate laser powers approaching saturation levels are used, for example, to acquire sufficient photon numbers when observation times are limited. The procedure involves use of a modified function for curve-fitting the ACF, but there are no additional fitting parameters. Instead, a simple calibration of the total fluorescence count rate as a function of relative laser power is fit to a polynomial, and the non-linear components of this fit, together with the relative laser power used for the FCS measurement, are used to specify the magnitude of additional terms in the fitting function. Monte Carlo simulations and experiments using Alexa dyes and quantum dots, with continuous and pulsed laser excitation, demonstrate the application of the modified fitting procedure with first order correction terms, in the regime where distortions in the ACF due to photobleaching and detector dead time are small compared to those of fluorescence saturation and triplet photophysics.

Keywords: fluorescence correlation spectroscopy; saturation; triplet; single-molecule detection; autocorrelation; artifacts; simulations; confocal microscopy.

1. INTRODUCTION

Fluorescence correlation spectroscopy (FCS) [1,2] is now a well established technique that is widely used for determining concentrations and kinetics of labeled molecules in a variety of applications, including homogeneous solution assays for pharmaceutical drug discovery [3,4], studies of molecular diffusion [5], conformational fluctuations [6], crowded molecular environments [7], and intracellular [8], interface [9] and membrane biophysics [10]. A few interesting recent reports include the use of FCS for an improved assay for 'mad cow disease' [11], a cost-effective FCS apparatus for use in teaching laboratories [12], tracking FCS of a single-particle [13], and a means of studying anomalous diffusion and lipid rafts in membranes by variation of the size of the focused laser beam [14,15,16,17]. Recent reviews have been published on the historical development [18,19], recent innovations [20] and biological and chemical applications [21,22]. FCS was first established in the early 1970's [23,24,25,26] as an extension of photon correlation spectroscopy methods for determination of particle diffusion kinetics by dynamic light scattering [27]. However, the widespread use of FCS as a routine tool for bioscience investigations has become possible only since subsequent improvements in signal-to-noise, with technical developments such as the demonstration of single-molecule detection in solution [28], the use of confocal microscopy with a high numerical aperture (NA) objective to reduce the sample volume [29,30], and the application of high quantum-efficiency single-photon avalanche-diode (SPAD) detectors [31,32].

In his review [18], Webb states that "FCS is now so efficient and sensitive that it can generate misleading data (if one is not meticulously careful about experimental design) faster than any other spectroscopy I know." Because of this realization, several research efforts have aimed to understand systematic errors, which can originate from numerous sources, and to present methodologies for avoiding or correcting such errors [33].

In general, systematic errors arise when the fitting function for the experimentally measured background-subtracted normalized autocorrelation function (ACF) of the total signal, $S(t)$,

$$g(\tau) = \langle S(t)S(t+\tau)\rangle / \left(\langle S(t)\rangle\langle S(t+\tau)\rangle\right) - 1, \quad (1)$$

does not accurately represent all of the physical processes that contribute to the experimentally acquired ACF. One may try to adjust the experimental set up to avoid these processes, or when this is not possible, filter their effects from the data, or modify the fitting function to account for the processes.

Systematic errors can arise if other sources of fluctuations such as laser power fluctuations are present [18], if there is a corruption of the photon data due to effects such as detector dead time [34] or afterpulses [35,36], or if approximations that the correlator makes in determining the experimental ACF from the photon data stream become poor [37,38,39]. Systematic errors can also arise if the shape of the probe region from which fluorescence is collected (which is defined by the focused laser and the optical collection system) differs from that modeled by the fitting function [40]. In the commonly-used confocal epi-illumination optical set up, the probe region is usually assumed to have a 3-dimensional (3-D) ellipsoidal Gaussian profile, with $1/e^2$ radius ω_0 and depth z_0. This shape is assumed in part because it yields a simple analytical form for the fitting function [41] (see Section 6 for derivation):

$$g_f(\tau) = N^{-1}(1+\tau/\tau_D)^{-1}(1+\zeta\tau/\tau_D)^{-1/2}, \quad (2)$$

where N is $3\sqrt{\pi}/4$ times the mean number of molecules contained within an ellipsoid (with abrupt-boundary) with radius ω_0 and depth $z_0 = \zeta^{-1/2}\omega_0$ [42], and $\tau_D = \omega_0^2/4D$ is the diffusional residence time, that is the mean (i.e., $1/e$) time that a molecule that begins at the origin remains within a sphere of radius ω_0. To reduce the number of fitting parameters, the confocal parameter ζ is usually determined independently, by curve fitting the ACF measured with a well characterized solution. Also, when background is present, N in Eqn. (2) is replaced by $N\left(1+B/\langle S\rangle\right)^2$, where B is the background count rate and $\langle S\rangle = \langle F\rangle + B$ is the total fluorescence plus background count rate [43].

Monte Carlo simulations [3,34,39,44,45,46,47,48,i] and numerical calculations [49,50,51,52,53,54,55,56] (which are also referred to as 'simulations' by some authors) have provided invaluable tools for quantitatively studying distortion and errors in the experimental ACF. Ref. [56] points out that in the widely used Zeiss Confocor 2 instrument [57], the laser beam overfills the microscope objective pupil and thus the focused beam is no longer strictly Gaussian. In consequence, the ACF will become distorted, but improved results can be obtained by use of a fitting function that uses numerical integration over the numerically calculated probe region profile. Ref. [56] calculates that a slight misalignment of the *z*-focus of the pinhole in this instrument can render the probe volume 3D-Gaussian once more, and hence suggests that the reason that the bias predicted by Ref. [40] is not observed in a subsequent study to characterize such bias [58] may be because of slight misalignment.

Pipetting errors and change of sample concentration due to chemical degradation, photobleaching [49,55], evaporation, or adsorption of molecules to glass surfaces can also lead to systematic errors and present difficult challenges when attempting to gain quantitative comparison between FCS and other analysis methods [59]. Detergents are often used to prevent sample adsorption to glass surfaces, but partitioning of fluorescent species into micelles can lead to changes in fluorescence properties (particularly in FRET-based assays) that may also account for observed systematic errors [59].

2. EFFECTS OF TRIPLET PHOTOPHYSICS AND SATURATION

In this article, we are primarily concerned with systematic errors that arise from excitation saturation, including saturation that results from triplet kinetics or other photophysical processes that cause the fluorophore to enter a dark state, such as photo-isomerization [60], as observed for the popular dye Cy5

[i] Dix, J.A.; Hom, E.F.Y. and Verkman, A.S. (2005) *Biophys. J.* **88**(1), 655A-655A Part 2 Suppl. S.

[61]. As the laser power is gradually increased so as to obtain adequate signal and acceptable data collection times, these effects are usually the first cause for distortion of the shape of the ACF away from the ideal form given by Eqn. (2). Triplet and saturation effects have been studied by several groups [3,33,46,47,48,49,50,51,52,53,54,55,56,62,63] and several methods for accounting for saturation in the ACF fitting function have been proposed in the literature [48,52,64,65].

Widengren, *et al.* [62,63] have conducted seminal studies of the effects of triplet photophysics in FCS for the case of continuous wave laser excitation. They solve the rate equations for a 3-level fluorescent molecule to determine the population dynamics for a molecule in a state of steady illumination. The level of illumination varies across the focused laser beam profile, but because the time constant at which molecules enter and leave the dark triplet state is generally much faster than the diffusional residence time τ_D, the adiabatic approximation can be used. That is, the effects of the triplet kinetics can usually be treated separately from diffusion in two time regimes—a fast time range, where molecules can be assumed to be immobile while triplet transitions occur, and a slow time range, where the triplet kinetics attain a steady state while the fluorophores diffuse. In the fast time range, $\tau << \tau_D$, where molecules are immobile at different parts of the beam, with different levels of illumination and hence different rates of triplet blinking, a weighted average is taken of the temporal dynamics over the beam profile, resulting in a multiplicative correction factor with a single exponential time constant. That is, to account for fast triplet blinking, Eqn. (2) is multiplied by a correction factor of the form

$$H(\tau) = A\exp(-\tau / \bar{\tau}_T) + 1, \tag{3}$$

where $A = \bar{T}/(1-\bar{T})$ with $\bar{T}$ equal to the averaged fraction of molecules within the probe region that are in the triplet state, and $\bar{\tau}_T$ can be roughly described as the averaged time constant for which molecules are driven into the triplet state. Note that the correction term is functionally the same as that for a fluorescent molecule A^* in a chemical equilibrium with a dark state B ($A^* \leftarrow (k_A, k_B) \rightarrow B$), where $\bar{T}$ represents the fraction in the dark state, and $\bar{\tau}_T = (k_A + k_B)^{-1} << \tau_D$ is independent of the laser illumination [27].

Ref. [63] does not provide an analytical expression for a correction term in the slow time range, but it does discuss the saturation effects that triplet kinetics cause, including a broadening of the probe volume away from the ideal Gaussian profile. Because it is mostly concerned with characterizing the fast time-scale triplet kinetics, rather than the various effects such as saturation that influence the amplitude of the ACF, it presents experimental ACF renormalized to an amplitude of $g(0) = 2$. However, it does use a freely-adjustable sum of two components with arbitrary values of τ_D to provide flexibility in curve fitting experimental ACF, in order to account for "wings" in the probe region that might arise from saturation or photobleaching effects.

Eqn. (3), or a similar factor [56],

$$H'(\tau) = (1-\xi)\exp(-\tau / \tau_T) + \xi, \tag{4}$$

with ξ and τ_T as fitting parameters, is widely used in the FCS literature to account for triplet kinetics, while the concomitant saturation effects are usually neglected. Note that the factor given by Eqn. (3) is always greater than 1 (for all τ), while the factor in Eqn. (4) is always less than or equal to 1. Fig. 3 of Ref. [3] shows that due to the simultaneously occurring saturation effects, the change in the ACF due to triplet kinetics can yield a correction factor that can be greater than 1 for small τ and at the same time smaller than 1 for large τ, depending upon the particular molecular parameters. This conclusion is obtained using an *ab-initio* Monte Carlo simulation of FCS, where photobleaching and other causes for distortion may be easily turned off.

Simulations show that if triplet crossing is "turned off", excitation saturation effects will still occur due to the finite fluorescence lifetime, which causes a decrease in the population of the ground-state of the fluorophore with increasing laser power, and leads to a clear decrease in the amplitude of the ACF (i.e., N appears to increase) and a small increase in ACF decay time (i.e., τ_D appears to increase)[ii,iii]. That is, distortion of the ACF due to excitation saturation will occur even if triplet crossing is negligible, although triplet effects accentuate saturation distortion. Similar observations have been reported in the literature by others [46]. The amplitude and decay time of the ACF is dependent on laser power, but Eqns. (2) and (3) do not provide for any power dependence. Although the measured ACF may still be fit with Eqns. (2) and (3), the apparent values obtained for N and τ_D will be increasingly biased as the laser power is increased. If saturation effects are not accounted for, then it can mistakenly seem that increased laser power causes partial optical trapping of molecules [66].

The numerical calculations presented in Ref. [56] for the case of saturation with continuous-wave laser excitation (where the scaling of the fluorescence signal F with laser irradiance I is given by $F \propto I/(1+I/I_S)$, where I_S is the saturation irradiance [67]) lead the authors to make a poignant observation: The dependence of the apparent N and τ_D values (obtained by curve fitting experimental ACF by Eqn. (2)) is greatest in the limit of low laser power. That is, it is not that bias occurs only if the laser power is above a threshold 'saturation' value, but rather, to obtain unbiased values for N and τ_D, one needs to extrapolate the results of a series of measurements to the case of zero laser power. Such extrapolation is time consuming, because acquisition of a series of ACF with comparable signal-to-noise requires roughly quadratically longer collection times as the laser power is decreased [56].

3. ACCOUNTING FOR SATURATION IN FITTING THE ACF

From a practical perspective, for many applications of FCS, including intracellular studies and pharmaceutical drug-binding assays, it is desirable to reduce the measurement time, rather than work with the lowest possible laser power. In order to obtain adequate photon statistics and signal-to-noise for short measurement durations, it is therefore desirable to increase the photon count rate by increasing the laser power. However, as described above, when even modest laser powers are used, saturation causes the ACF to change its amplitude and shape. Therefore, it is desirable to find simple modifications to the ACF fitting function to account for the power dependence.

A modified fitting function has previously been introduced to account for saturation in ACF data collected at high laser powers in 2-photon excitation experiments [64,65]. However, this fitting function is obtained with the assumption that saturation has an abrupt onset and causes the probe region to have a flat-top shape. Ref. [50] points out that the assumed shape "has no physical meaning and introduces fictitious parameters". The fitting function includes an additional quantity, α, which is essentially an empirical parameter that lends added flexibility for better fitting of the saturation-distorted ACF data. Further, α must be determined by globally fitting a set of ACF, which itself requires some time to collect.

Ref. [52] presents another method for accounting for saturation effects by scaling the adjustable parameters (N, τ_D, ζ) in the fitting function given in Eqn. (2) by three factors, which are numerically calculated using a physical model of saturation. These factors are all dependent on a quantity R_{sat}, which equals the laser irradiance divided by a parameter I_{sat}, that once more must be determined by globally fitting a set of ACF. This procedure yields self-consistent values for experimental 2-photon excitation results with Rhodamine 6G over the range of laser powers, when an additional term with two adjustable parameters is included to account for photobleaching.

[ii] Davis, L.M.; Ball, D.A.; Williams, P.E.; Swift, K.M. and Matayoshi, E.D. (2003) in *Picoquant 9th International Workshop on 'Single Molecule Detection and Ultra Sensitive Analysis in the Life Sciences'*, Berlin, Germany; http://ldavis.utsi.edu/PDFs/2003-picoquant1.pdf.

[iii] Davis, L.M.; Shen, G.Q. and Ball, D.A. (2004) in *Focus on Microscopy 2004*, Philadelphia, PA.

We recently reported another method for accounting for saturation effects when fitting the ACF and demonstrated this method using Monte Carlo simulations of FCS with continuous-wave (cw) excitation and no triplet kinetics [48]. The method, which is applicable to one or two-photon excitation, with pulsed or cw excitation, is simple to apply, and does not require one to collect a series of ACF over a range of laser powers. Instead, only the fluorescence count rate as a function of relative laser power, for the particular experimental configuration and sample, needs to be measured to 'calibrate' the effects of saturation. Despite its simplicity, the new laser-power-dependent ACF fitting function is derived from a detailed theoretical model of the molecular photophysics, which we present below in a form that now also includes the triplet correction factor of Eqn. (3). While the theoretical derivation yields new insight into the nature of saturation effects and its differences for various forms of laser excitation, readers who wish to skip ahead to the application of the theory may turn to Section 7.

4. FLUORESCENCE SATURATION BEHAVIOR

In this section, we discuss the physical processes that occur following excitation of a fluorescent molecule in terms of a rate equation model. Such models have been previously used to provide a better understanding of saturation in FCS [46,48,49,51,55]. Here we discuss the time scales of the various photophysical processes for typical fluorophores in solution, to derive a unified explanation of saturation effects for cw excitation, pulsed one-photon excitation, and two-photon excitation. While the differences in the saturation behavior are noteworthy, in all cases, a simple Taylor series expansion may be made of the dependence of the fluorescence on laser power, although for cw excitation the expansion only converges for laser powers below a critical value.

For one-photon excitation, either a cw laser beam or a train of sub-nanosecond pulses is used for sample excitation. However, for two-photon excitation, a train of pulses of duration ~100 femtosecond is usually used in order to attain adequate peak irradiance. The different timescales of the laser pulses and the physical processes that occur as a result of molecular excitation [68], which are indicated in Fig. 1 (a), give rise to different saturation behavior for one- and two-photon excitation and for pulsed and cw excitation.

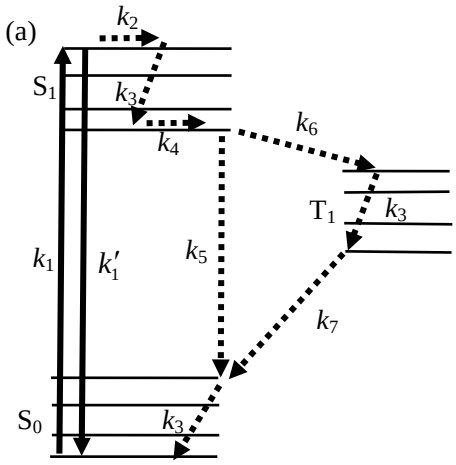

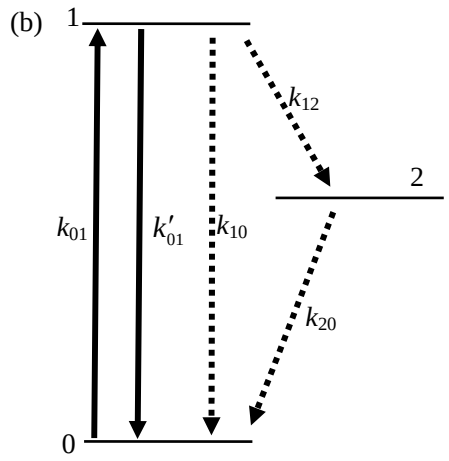

Fig. 1: (a) Typical timescales of molecular processes: k_1: one or two-photon excitation; k_1': one or two-photon stimulated emission; k_2: collisional dephasing (~10 fs); k_3: vibrational thermalization (~1 ps); k_4: rotational reorientation (~100 ps—100 ns); k_5: fluorescence (~2 ns); k_6: inter-system crossing (~200 ns); k_7: phosphorescence (~1 μs); (b) Simplified 3-level scheme, in which only the electronic levels are retained.

After an organic dye molecule is excited (at a rate k_1 shown in Fig. 1 (a)) to a particular sublevel of the S_1 excited state manifold, its electronic wavefunction becomes dephased due to elastic collisions with solvent molecules within a timescale of k_2^{-1}~10 fs, which is typically much faster than the laser excitation pulsewidth, and hence coherence effects are usually negligible and the optical Bloch equations that describe the system are well approximated by rate equations [69]. After dephasing, thermal relaxation within the S_1 excited state manifold due to inelastic collisions with solvent molecules occurs within a timescale of k_3^{-1}~1 ps. Reorientation of the transition dipole moment due to rotational diffusion of the molecule may also occur on a timescale of k_4^{-1} ~100 ps for a small dye molecule in aqueous solution and with k_4^{-1} up to ~100 ns for a chromophore rigidly bound to a macromolecule. Fluorescence and/or internal conversion back to the S_0 ground state manifold then occur within about k_5^{-1} ~2 ns. Intersystem crossing to the triplet T_1 manifold is a competing process, which typically occurs about 1 in 100 times, and thus with k_6^{-1}~200 ns. In typical oxygen-saturated aqueous solutions, relaxation from triplet T_1 back to the ground S_0 manifold then occurs within about k_7^{-1} ~1 μs. Because of the disparate timescales of the molecular processes described above, the molecular energy level system in Fig 1 (a) is well approximated by the 3-level system shown in Fig. 1 (b), with $k_1 \to k_{01}$, $k_1' \to k_{01}'$, $k_5 \to k_{10}$, $k_6 \to k_{12}$, $k_7 \to k_{20}$.

For cw excitation, saturation occurs primarily as a result of the decrease in the fractional population N_0/N of the ground state 0 with increasing laser irradiance. The laser pumps molecules from the ground state 0 to the excited singlet state 1, but the stimulated emission pumping from 1 to 0, k_{01}' is negligible, because $k_3 >> k_1$ in Fig. 1 (a). The rate equations for the 3-level system may then be expressed as

$$\frac{d}{dt}\begin{pmatrix} N_0 \\ N_1 \\ N_2 \end{pmatrix} = \begin{pmatrix} -k_{01} & k_{10} & k_{20} \\ k_{01} & -k_{10}-k_{12} & 0 \\ 0 & k_{12} & -k_{20} \end{pmatrix}\begin{pmatrix} N_0 \\ N_1 \\ N_2 \end{pmatrix}, \tag{5}$$

which has the steady state solution

$$\begin{pmatrix} N_0 \\ N_1 \\ N_2 \end{pmatrix} = \begin{pmatrix} k_{10} + k_{12} \\ k_{01} \\ k_{01}k_{12}/k_{20} \end{pmatrix} \times \frac{N}{k_{10} + k_{12} + k_{01}(1 + k_{12}/k_{20})}, \tag{6}$$

where N_j/N is the fractional population of level j, with $N = \sum N_j$. Here, the cw excitation rate is

$$k_{01} = \sigma_a \langle I \rangle / E_r, \tag{7}$$

where σ_a is the absorption cross-section (equal to 3.82×10^{-21} cm^{3}M times the molar absorptivity), $\langle I \rangle$ is the cw laser irradiance, and E_γ is the laser photon energy. The mean fluorescence count rate from a single molecule, which is proportional to the decay rate k_{10}, and the fractional excited state population N_1/N, obtained from the second line of Eqn. (6), is given by

$$F = \frac{Ck_{10}}{1+Q} \frac{\langle I \rangle / I_S}{1 + \langle I \rangle / I_S}, \tag{8}$$

where C is the net collection and detection efficiency (including fluorescence quantum efficiency), the saturation irradiance I_S is given by

$$I_S = 1/(\eta(1+Q)), \tag{9}$$

where η is defined by

$$\eta = \sigma_a \tau_F / E_r, \tag{10}$$

$$\tau_F = (k_{10} + k_{12})^{-1} \tag{11}$$

is equal to the fluorescence lifetime, and

$$Q = R\tau_P / \tau_F, \tag{12}$$

in which $R = k_{12}/(k_{10} + k_{12})$ is the triplet crossing yield, and $\tau_P = k_{20}^{-1}$ is the phosphorescence lifetime.

For repetitively pulsed excitation, a major factor that contributes to saturation is ground state depletion during the course of each laser excitation pulse. The nature of this process will depend upon if the pulsewidth δt is shorter or longer than the S_1 thermalization time k_3^{-1} in Fig. 1(a). If the pulsewidth is longer than $k_3^{-1} \sim 1$ ps, stimulated emission pumping from 1 to 0 can be neglected, because the S_1 manifold relaxes during the course of each pulse, and hence the situation during each pulse is the same as that in Eqn. (5). With the assumption that the duration of the laser pulse δt is short compared to the fluorescence lifetime ($\delta t << \tau_F$), the decay of the excited state and triplet populations during the interval of the laser pulse $0 < t < \delta t$ can be ignored and the top line of Eqn. (5) gives

$$dN_0 / dt = -k_{01} N_0, \qquad \text{(during pulse)} \tag{13}$$

which has the solution

$$N_0(\delta t) = N_0(0)\exp(-k_{01}\delta t)\,, \qquad (\text{for } k_3^{-1} << \delta t << \tau_F) \tag{14}$$

in which k_{01} is defined in Eqn. (7) with $\langle I \rangle$ replaced by $\bar{I}$, where $\bar{I}$ equals the mean irradiance during the laser pulse, given by $\bar{I} = \int_0^{\delta t} I(t)dt \Big/ \delta t$. (Ref. [51] provides details on the case of $I(t)$ equal to a Gaussian.) However, when the laser excitation pulsewidth is shorter than $k_3^{-1} \sim$ 1 ps, as it typically is for two-photon excitation, laser physics theory [70] states that the laser not only excites the molecule, but for high irradiance it can drive the excited molecule back to the ground state by stimulated emission (as indicated in Fig. 1(b) by the downward transition at rate k'_{01}), because the excited levels within the S_1 manifold do not have time to thermalize, so that Eqn. (13) must be replaced by

$$dN_0 / dt = -k_{01}N_0 + k'_{01}N_1\,, \qquad (\text{during pulse}). \tag{15}$$

Here, $k'_{01} = (g_0 / g_1)k_{01}$, where the g's are the degeneracies or density of levels in the S_0 and S_1 manifolds. The time after excitation until the next laser pulse, T, is much greater than the time required for thermalization of the excited state manifold $k_3^{-1} \sim$1 ps and hence $N_1(0) \approx 0$, so that the solution of Eqn. (15) is

$$N_0(\delta t) = N_0(0)\kappa^{-1}\left(\exp(-\kappa k_{01}\delta t) + \kappa - 1\right), \qquad \text{for } k_2^{-1} << \delta t << k_3^{-1}, \tag{16}$$

where $\kappa = (g_0 + g_1) / g_1$. A comparison of Eqns. (14) and (16) shows that theory predicts a difference in the saturation behavior as the pulse length becomes shorter than the ~1 ps time for thermalization of the S_1 manifold, due to the role of stimulated emission, but the equations become the same if $\kappa \to 1$.

After the laser pulse, the molecule relaxes from the excited state 1. The solution of Eqn. (5) with $k_{01} = 0$ can then be used with the initial condition of Eqn. (14) or (16) and the periodicity condition $N_j(T) = N_j(0)$, to determine the dependence of the mean fluorescence count rate

$$\langle F \rangle = \int_0^T F(t)dt \Big/ T \tag{17}$$

on the average laser irradiance

$$\langle I \rangle = \bar{I}\delta t / T\,. \tag{18}$$

A similar procedure for determining the time-averaged fluorescence with repetitively pulsed excitation is described in Ref. [55].

For pulsed excitation, the solution obtained in this way with the initial condition of Eqn. (16) yields

$$\langle F \rangle = Ck_{10}\frac{\tau_F}{T}a\frac{1 - \exp(-\langle I \rangle / I'_S)}{c - b\exp(-\langle I \rangle / I'_S)}\,, \tag{19}$$

where $a = (1 - \exp(-T / \tau_F))$, $b = Q' + \exp(-T / \tau_F)$, and $c = b + a\kappa$, which simplifies to

$$\langle F \rangle \approx Ck_{10}\frac{\tau_F}{T}\frac{1 - \exp(-\langle I \rangle / I'_S)}{\kappa + Q'(1 - \exp(-\langle I \rangle / I'_S))}, \qquad \text{for } \tau_F << T\,, \tag{20}$$

where

$$I'_S = (\eta\kappa T / \tau_F)^{-1}, \tag{21}$$

and

$$Q' = R\frac{\tau_P}{\tau_P - \tau_F}\frac{\exp(-T/\tau_P) - \exp(-T/\tau_F)}{1-\exp(-T/\tau_P)} \tag{22}$$

$$\approx R\frac{\tau_P}{T}, \qquad \text{for } \tau_F << T << \tau_P \ . \tag{23}$$

For the typical values of R ~10^{-2}, τ_P ~1 μs, T ~10 ns, Eqn. (23) gives Q' ~1 and Eqn. (20) shows that near saturation triplet shelving reduces the mean fluorescence signal by up to ~50%. The case of excitation with pulsewidths greater than ~1ps is found by setting $\kappa \to 1$.

For two-photon excitation, Eqn. (7) is replaced by

$$k_{01} = \sigma_{TPF}\overline{I^2}\Big/E_r^2 \ , \tag{24}$$

in which $\overline{I^2} = \int_0^{\delta t} I^2(t)dt\Big/\delta t$ and σ_{TPF} is the two-photon absorption cross-section, typically expressed in units of GM=10^{-50} cm^4 s. Note that Eqn. (24) is a classical approximation and σ_{TPF} should be regarded as an effective parameter for the particular detailed photon statistics (i.e., the second order quantum mechanical coherence function of the light), which will depend on the shape, chirp, and coherence of the pulse [71]. Thus, for two-photon excitation, Eqns. (19) and (20) may still be used but with $\langle I \rangle$ replaced by

$$\langle I^2 \rangle = \overline{I^2}\delta t\Big/T \tag{25}$$

and I_S' replaced by

$$I_S'' = \left(\eta''\kappa T\Big/\tau_F\right)^{-1}, \tag{26}$$

where

$$\eta'' = \sigma_{TPF}\tau_F\Big/E_r^2 \ . \tag{27}$$

Eqns. (8) and (19) may be approximated by Taylor expansions in $\langle I \rangle$ to yield

$$\langle F \rangle = C\sum_{n=1}^{\infty}\alpha_n\left(\langle I \rangle / I_S\right)^n, \tag{28}$$

where

$$\alpha_n = -k_{10}(-1)^n/(1+Q), \tag{29}$$

for cw excitation with $\langle I \rangle < I_S$,

$$\alpha_n = -k_{10}(\tau_F/(\kappa T))(-1)^n/n!, \tag{30}$$

for pulsed excitation, with $Q' = 0$, $\tau_F << T$, $I_S \to I_S'$, or $I_S \to I_S''$.

Note that for cw excitation, the fluorescence rate in Eqn. (8) may be expressed as a binomial expansion of $(1+x)^{-1}$, where $x = \langle I \rangle / I_S$, which is valid and converges only for $\langle I \rangle < I_S$ (see page 261, Ref. [67]). However, for pulsed excitation (with pulsewidth δt within the bounds $k_3^{-1} << \delta t << \tau_F$), the power series expansion always converges. If $Q' = 0$ (i.e., no triplet) the fluorescence rate in Eqn. (20) simplifies, and may be easily expanded as an exponential series, with coefficients given in Eqn. (30), which clearly converges for all $\langle I \rangle$. For the general case of pulsed excitation, Eqn. (19) may first be expressed in terms

of a binomial expansion of $(1-y)^{-1}$, in which $y=(b/c)\exp(-\langle I\rangle/I_S)$. This is seen to converge for all $\langle I\rangle$, as $y<1$. When the exponential term in y is expanded and the equation regrouped, we find

$$\alpha_n = -k_{10}\frac{\tau_F}{T}a(1/b-1/c)(-1)^n\sum_{m=0}^{\infty}m^n(b/c)^m \Big/ n!, \qquad (31)$$

for pulsed excitation, with $I_S \to I_S'$, or $I_S \to I_S''$.

Fig. 2 illustrates the differences between Eqns. (8), (20) with $\kappa\to 1$, and (20) with $\kappa = 2$ for the case of no triplet, $Q'=0$, and also a comparison with the Taylor expansions of Eqns. (28)—(30) in which only the first two terms are kept. Note that the signal rate at which excitation saturation occurs is lower for pulsed excitation than for cw excitation, and is lower still for excitation with sub-picosecond pulses, as is typically used for two-photon excitation. For cw excitation, the first two terms of the Taylor approximation are adequate for $\langle I\rangle/I_S < \sim 0.2$.

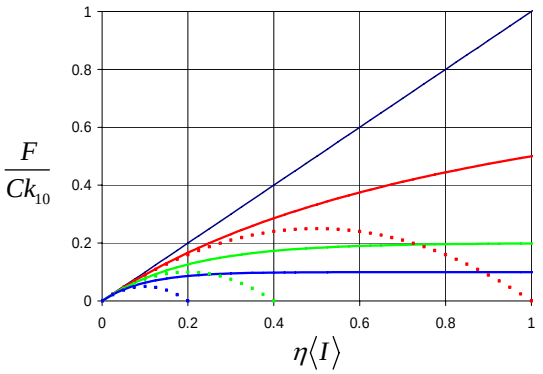

Fig. 2: F/Ck_{10} vs. $\eta\langle I\rangle$ as calculated for cw excitation by Eqn. (8) with Q = 0 (red; top); for sub-nanosecond pulsed excitation by Eqn. (20) for $Q'=0$, $T/\tau_F=5$ and $\kappa\to 1$, (green; middle); and for sub-picosecond pulsed excitation by Eqn. (20) for $Q'=0$, $T/\tau_F=5$ and $\kappa=2$, (blue; bottom). The dashed curves show the corresponding Taylor expansions of Eqns. (28)—(30) with just the first two terms kept.

In order to experimentally demonstrate the different saturation behavior between cw and pulsed laser excitation, measurements were made of the mean fluorescence count rate versus laser power for an 11.4 μM solution of Rhodamine B in water using 532 nm 70ps/76MHz pulsed excitation and 514 nm cw excitation. For these experiments, the incoming laser beam considerably under-filled the microscope objective to ensure that the beam was not tightly focused in the sample and the fluorescence was collected only from the central region of the focused beam by use of a small pinhole as a spatial filter. Under these conditions, there should be little spatial averaging over the irradiance profile of the laser, and the fluorescence count rates are expected to directly follow the shape of Eqn. (8) for cw and Eqn. (19) (with $\kappa\to 1$) for sub-nanosecond pulsed excitation. Fig. 3 compares fluorescence counts versus laser power normalized by the solution absorption at each wavelength used, for 532 nm 70ps/76MHz pulsed excitation (Coherent, Antares frequency-doubled Nd:YAG laser) and 514 nm cw excitation (Spectra Physics, 2060-10S BeamLok Argon-ion laser). The results illustrate a key point that the fluorescence rate at which excitation saturation occurs is lower for pulsed excitation than for cw excitation.

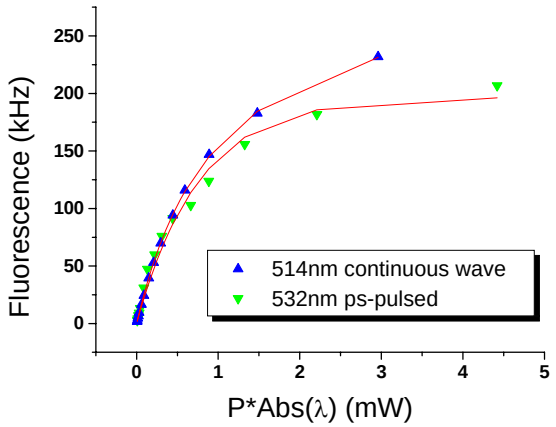

Fig. 3: Experimental measurements of the fluorescence count rate versus laser power, normalized by the absorptivity at the used wavelength, illustrating differences in the onset of saturation for continuous wave (514 nm) and pulsed (532 nm, 70 picosecond) irradiation. The red curves are fits to the functional forms of Eqns. (8) and (20) respectively.

5. GAUSSIAN APPROXIMATION TO THE FLUORESCENCE PROFILE WITH SATURATION

For a Gaussian laser beam focused by a moderate NA microscope objective, the irradiance profile near the focus is

$$I(x,y,z) = \frac{2P}{\pi\omega_0^2\left(1+(z/z_0)^2\right)}\exp\left(\frac{-2(x^2+y^2)}{\omega_0^2\left(1+(z/z_0)^2\right)}\right), \tag{32}$$

where P is the laser power, ω_0 is the beam waist, the Rayleigh range is

$$z_0 = n_0\pi\omega_0^2/\lambda_0\,, \tag{33}$$

n_0 is the refractive index of the solvent, and λ_0 is the vacuum wavelength of the laser. Moreover, for $z << z_0$,

$$\begin{aligned} I(x,y,z) &\approx \frac{2P}{\pi\omega_0^2}\exp\left(\frac{-2(x^2+y^2)}{\omega_0^2}\right)\frac{1}{1+(z/z_0)^2} \approx \frac{P}{2\pi\sigma^2}\exp\left(\frac{-(x^2+y^2)}{2\sigma^2}\right)\exp\left(\frac{-z^2}{2\sigma_z^2}\right) \\ &\approx P\sqrt{2\pi}\sigma_z G(x,\sigma)G(y,\sigma)G(z,\sigma_z)\,, \end{aligned} \tag{34}$$

where

$$G(s,\sigma') = \frac{1}{\sqrt{2\pi}\sigma'}\exp\left(-\frac{s^2}{2\sigma'^2}\right) \tag{35}$$

is a Gaussian with standard deviation σ', normalized such that

$$\int_{-\infty}^{\infty} G(s,\sigma') = 1\,, \tag{36}$$

and where we have set

$$\sigma = \omega_0/2\,,\ \text{and}\ \ \sigma_z = z_0/\sqrt{2\ln 2}\,, \tag{37}$$

so that the half-width of the Lorentzian profile in z is matched to the half-width of the Gaussian approximation. Similarly, with

$$\left[1+(z/z_0)^2\right]^{-n} \approx G\left(z,\sigma_z/\sqrt{2^{1/n}-1}\right)\sqrt{2\pi}\sigma_z/\sqrt{2^{1/n}-1} \quad , \tag{38}$$

we have

$$I^n(x,y,z) \approx P^n(2\pi)^{3/2-n}n^{-1}\sigma^{2-2n}\sigma_z(2^{1/n}-1)^{-1/2}G\left(x,\sigma/\sqrt{n}\right)G\left(y,\sigma/\sqrt{n}\right)G\left(z,\sigma_z/\sqrt{2^{1/n}-1}\right). \tag{39}$$

The mean number of fluorescence photons per second detected from a single molecule located at x,y,z is given by Eqn. (8), or (19) with $\langle I \rangle$ replaced by $I(x,y,z)$, which is approximated by the 3-D Gaussian profile of Eqn. (34), and with C replaced by the collection efficiency function $C(x,y,z)$, which is also approximated to be 3D-Gaussian in shape [29],

$$C(x,y,z) = C_0(2\pi)^{3/2}\sigma_C^2\sigma_{Cz}G(x,\sigma_C)G(y,\sigma_C)G(z,\sigma_{CZ}) \, , \tag{40}$$

with C_0 equal to the peak collection efficiency, and σ_C , σ_{CZ} equal to the standard deviations in the radial and axial directions, as determined by the pinhole radius, and the magnification and numerical aperture of the microscope objective. Fig. 4 shows that as the laser irradiance increases, the fluorescence profile, numerically calculated by inserting Eqn. (32) into Eqn. (8) or (19) with $\kappa = 2$ (to model two-photon sub-picosecond excitation), does not attain the flat-top profile that was assumed in Refs. [64,65] for $C(x,y,z) = 1$.

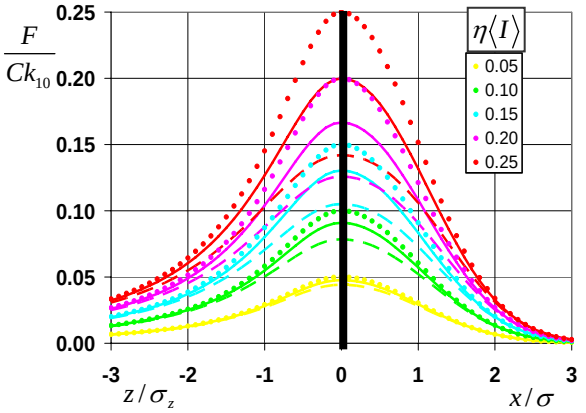

Fig. 4: Gaussian-Lorentzian irradiance profiles with no saturation (dotted), obtained from Eqn. (32), and the resulting fluorescence profiles with saturation, obtained using Eqn. (8) for cw excitation with $Q = 0$ (solid), and Eqn. (19) for pulsed excitation with $Q' = 0$, $T/\tau_F = 5$, $\kappa \to 1$ (dashed). The left side of the graph shows the axial profiles ($x = y = 0$) and the right side shows the radial profiles ($y = z = 0$), with $\eta I(0,0,0)$ = 0.05, 0.10, 0.15, 0.20, 0.25. Note that the saturated profiles do not have the "flat-top" profile that was assumed in Ref. [65] and which is seen from Ref. [51] to occur only for $\eta I(0,0,0) >> 1$.

Since the product of two Gaussian functions is another Gaussian,

$$G(s,\sigma_1)G(s,\sigma_1) = G(0,(\sigma_1^2+\sigma_2^2)^{1/2})G(s,(\sigma_1^{-2}+\sigma_2^{-2})^{-1/2}) \, , \tag{41}$$

Eqn. (28) may be used to express the fluorescence profile as a sum of 3-D Gaussian functions:

$$F(x,y,z) \approx \sum_{n=1}^{\infty}\Phi_n G\left(x,\overline{\sigma}(n)\right)G\left(y,\overline{\sigma}(n)\right)G\left(z,\overline{\sigma}_z(n)\right) \tag{42}$$

where

$$\Phi_n = \left(\alpha_n / I_S^n\right) C_0 P^n (2\pi)^{3/2-n} n^{-1} \sigma^{2-2n} \sigma_z (2^{1/n}-1)^{-1/2} \sigma_C^2 \sigma_{Cz} (\sigma_C^2 + \sigma^2/n)^{-1} (\sigma_{Cz}^2 + \sigma_z^2/(2^{1/n}-1))^{-1/2} \quad (43)$$

$$\overline{\sigma}(n) = (n\sigma^{-2} + \sigma_C^{-2})^{-1/2}, \quad (44)$$

$$\overline{\sigma}_z(n) = ((2^{1/n}-1)\sigma_z^{-2} + \sigma_{Cz}^{-2})^{-1/2}. \quad (45)$$

For cw excitation, as noted in Eq. (29), the summation in Eqn. (42) converges only for $P < \pi\omega_0^2 I_S/2$. The details of the functional dependence of the proportionality factors Φ_n is of little importance, except to note the power dependence and to later show how they may be experimentally determined and used to estimate the saturation irradiance. Hence Eqn. (42) is to be re-expressed

$$F(x,y,z) \approx \sum_{n=1}^{\infty} \chi_n \tilde{P}^n G(x,\overline{\sigma}(n)) G(y,\overline{\sigma}(n)) G(z,\overline{\sigma}_z(n)), \quad (46)$$

where $\tilde{P}$ is now the relative power of the laser beam, which can be measured before the FCS apparatus, rather than at the sample, and χ_n are empirical factors to be determined in calibration measurements, and

$$\Phi_n = \chi_n \tilde{P}^n. \quad (47)$$

For low laser power and no saturation, only the first term in the sum of Eqn. (42) or (46) needs to be retained and the profile is 3-D Gaussian. As the power is increased, the second term also must be retained. Other causes for distortion of the ACF must be accounted for before it would be useful to continue the power series beyond the second or third term. In particular, detector and electronic counting saturation, especially at higher particle concentrations, as discussed in Ref. [34], would need to be addressed.

6. DERIVATION OF FITTING FUNCTION FOR ACF WITH SATURATION

A derivation of the theoretical form of the ACF, Eqn. (2), in terms of intensity fluctuations due to diffusion-induced concentration-fluctuations is given in the early FCS literature [41]. Here we give a reformulated derivation in terms of single-photon detection from single-molecules, and this formulation is extended to account for saturation. Ref. [48] provides further details, including a derivation of the fitting function both with and without saturation, and provides results for flow transport and cross-correlations, but does not include triplet effects.

Let ρ be the number density of molecules, with dimensions of m^{-3}. Note that ρ also equals the probability density to find a single molecule at any location x,y,z. If the total signal $S(t)$ is a stationary ergodic random process, then the time averages in Eqn. (1) may be evaluated as ensemble averages and the average total rate of photons is independent of time and equals the fluorescence count rate averaged over all possible molecule locations plus background:

$$\langle S(t) \rangle = \iiint \rho F(x,y,z)\,dx\,dy\,dz + B \quad (48)$$

$$= \sum_{n=1}^{\infty} \rho\, \Phi_n + B, \quad (49)$$

$$= \sum_{n=1}^{\infty} \rho \chi_n \tilde{P}^n + B(\tilde{P}) \quad (50)$$

where B is the total background count rate, which may be dependent on the relative power $\tilde{P}$, and where we have substituted the Taylor series in Eqn. (42) and used Eqn. (36) to perform the integrations for each of

the dimensions x, y, z for each of the terms. As $S(t)$ is a stationary random variable, each of the two factors in the denominator of the first term of Eqn. (1) is given by Eqns. (48)-(50).

The term $S(t)S(t+\tau)$ in the numerator of Eqn. (1) is the rate of detection of pairs of photons that are separated by an interval τ. The first photon may arise from a single-molecule located at $\mathbf{r}_1 = x_1, y_1, z_1$, with probability density ρ, or background. The second photon may arise either from the same single-molecule, which has moved from $\mathbf{r}_1$, to $\mathbf{r}_2 = x_2, y_2, z_2$ during the time interval τ, with a probability density $M(\mathbf{r}_1 - \mathbf{r}_2, \tau)$ or from a different single-molecule, again with probability density ρ, or from background. The numerator of the first term of Eqn. (1) is thus:

$$\left\langle S(t)S(t+\tau)\right\rangle = \int \rho F(\mathbf{r}_1)d\mathbf{r}_1 \int M(\mathbf{r}_1 - \mathbf{r}_2, \tau)F(\mathbf{r}_2, \tau)d\mathbf{r}_2 + \left(\int \rho F(\mathbf{r}_1)d\mathbf{r}_1\right)^2 + 2B\int \rho F(\mathbf{r}_1)d\mathbf{r}_1 + B^2, \tag{51}$$

where

$$M(r,\tau) = G(x,\sigma_D(\tau))G(y,\sigma_D(\tau))G(z,\sigma_D(\tau)) \tag{52}$$

is the probability density for a molecule to diffuse from the origin to $\mathbf{r} = x, y, z$ at time τ, and

$$\sigma_D(\tau) = \sqrt{2D\tau}. \tag{53}$$

Eqn. (52) is the solution of the diffusion equation

$$\partial\rho / \partial t = D\nabla^2\rho \tag{54}$$

for the initial condition of a molecule located at the origin, $\rho(x,y,z,0) = \delta(0,0,0)$, where $\delta(0,0,0)$ is a 3-D Dirac delta function, and D is the diffusion coefficient. In Eqn. (51), the term $M(\mathbf{r}_1 - \mathbf{r}_2, \tau)F(\mathbf{r}_2, \tau)$ accounts for the probability density to detect a photon at time τ from a molecule at $\mathbf{r}_2$ that has diffused from $\mathbf{r}_1$, after emitting a photon at time 0. Following Ref. [63], we have invoked the adiabatic approximation to allow the diffusion and molecular photokinetics to be factored, and we approximate

$$F(\mathbf{r}_2, \tau) \approx F(\mathbf{r}_2)\left(1 + A\exp(-\tau / \bar{\tau}_T)\right), \tag{55}$$

where $\bar{\tau}_T$ is defined after Eqn. (3), and A is an empirical value to be determined when fitting the ACF. The interpretation of Eqn. (55) is that after a molecule has emitted a photon at time 0, it begins in the ground state, and hence there is an enhanced probability of fluorescence until the probability that the molecule occupies the triplet state reaches a steady state. The steady state is reached in a mean time $\bar{\tau}_T \approx \left\langle k_{20}\left(1 + QI(\mathbf{r})/I_S\right)\right\rangle$ and $A \approx \left\langle QI(\mathbf{r})/I_S\right\rangle$, where the angular brackets denote an average over the probe region. Thus the first term on the right hand side of Eqn. (51) is

$$J = \left(1 + A\exp(-\tau / \bar{\tau}_T)\right)\rho \int F(\mathbf{r}_1)d\mathbf{r}_1 \int M(\mathbf{r}_1 - \mathbf{r}_2, \tau)F(\mathbf{r}_2)d\mathbf{r}_2 \,. \tag{56}$$

The Taylor expansions in terms of Gaussians from Eqn. (42) are substituted for $F(\mathbf{r}_1)$ and $F(\mathbf{r}_2)$ and the integrations may be performed separately for each dimension, as Eqn. (52) also factors into functions for each dimension. This yields

$$J = \left(1 + A\exp(-\tau / \bar{\tau}_T)\right)\rho \sum_{n=1}^{\infty}\sum_{m=1}^{\infty} \Phi_n \Phi_m \int G(x_1, \bar{\sigma}(n))dx_1 \int M(x_1 - x_2, \tau)G(x_2, \bar{\sigma}(m))dx_2$$

$$\times \int G(y_1, \bar{\sigma}(n))dy_1 \int M(y_1 - y_2, \tau)G(y_2, \bar{\sigma}(n))dy_2$$
$$\times \int G(z_1, \bar{\sigma}_z(n))dx_1 \int M(z_1 - z_2, \tau)G(z_2, \bar{\sigma}_z(n))dz_2 \qquad (57)$$

The integrations are convolutions of Gaussian functions. For the x-dimension, each integral term is

$$J_x(n,m) = \int dx_1 G(x_1, \bar{\sigma}(n)) \int dx_2 G(x_1 - x_2, \sigma_D(\tau))\, G(x_2, \bar{\sigma}(m)) \,. \qquad (58)$$

Since the convolution of two Gaussians is another Gaussian, with a width that is the sum in quadrature of the widths of the two,

$$\int dx G(x, \sigma_1) G(x \pm x', \sigma_2) = G(x', \sqrt{\sigma_1^2 + \sigma_2^2}) \,, \qquad (59)$$

we find

$$J_{x|y}(n,m) = G\left(0, \sqrt{\bar{\sigma}^2(n) + \bar{\sigma}^2(m) + \sigma_D^2(\tau)}\right)$$
$$= G\left(0, \sqrt{(\alpha_{nm} + \tau/\tau_D)/2}\right) \Big/ \bar{\omega}_0 \,, \qquad (\text{as } G(as, a\sigma) = G(s,\sigma)/a)$$
$$= \pi^{-1/2} \bar{\omega}_0^{-1} \left(\alpha_{nm} + \tau/\tau_D\right)^{-1/2} , \qquad (60)$$

and similarly

$$J_z(n,m) = \pi^{-1/2} \bar{z}_0^{-1} \left(\beta_{nm} + \bar{\zeta}\tau/\tau_D\right)^{-1/2} , \qquad (61)$$

with

$$\alpha_{nm} = \left(\bar{\sigma}^2(n) + \bar{\sigma}^2(m)\right) \Big/ \left(2\bar{\sigma}^2(1)\right), \qquad (62)$$

$$\beta_{nm} = \left(\bar{\sigma}_z^2(n) + \bar{\sigma}_z^2(m)\right) \Big/ \left(2\bar{\sigma}_z^2(1)\right), \qquad (63)$$

$$\tau_D = \bar{\omega}_0^2 / 4D \,, \qquad (64)$$

$$\bar{\zeta} = (\bar{\omega}_0 / \bar{z}_0)^2 \,, \qquad (65)$$

$$\bar{\omega}_0 = 2\bar{\sigma}(1) = 2(4\omega_0^{-2} + \sigma_C^{-2})^{-1/2} \,, \qquad (66)$$

$$\bar{z}_0 = 2\bar{\sigma}_z(1) = 2(4z_0^{-2} + \sigma_{Cz}^{-2})^{-1/2} \,. \qquad (67)$$

Substituting (60) and (61) into Eqn. (57) yields

$$J = \left(1 + A\exp(-\tau/\bar{\tau}_T)\right)\left(\rho \,/\, (\pi^{3/2} \bar{\omega}_0^2 \, \bar{z}_0)\right) \sum_{n=1}^{\infty} \sum_{m=1}^{\infty} \Phi_n \Phi_m \left(\alpha_{nm} + \tau/\tau_D\right)^{-1} \left(\beta_{nm} + \bar{\zeta}\tau/\tau_D\right)^{-1/2} . \qquad (68)$$

This is the first term on the right hand side of Eqn. (51). The last three terms of Eqn. (51) are equal to the square of Eqn. (49). The denominator of the first term in Eqn. (1) is also the square of Eqn. (49). Hence, when all is inserted into Eqn. 1, we obtain a fitting function given by Eqn. (68) divided by the square of Eqn. (49). With the use of Eqn. (47), this may be expressed as

$$g_f(\tau) = N^{-1}\left(1 + A\exp(-\tau/\bar{\tau}_T)\right)\sum_{n=1}^{\infty}\sum_{m=1}^{\infty}\rho^2\chi_n\chi_m\tilde{P}^{n+m}\left[\alpha_{nm} + \tau/\tau_D\right]^{-1}\left[\beta_{nm} + \bar{\zeta}\tau/\tau_D\right]^{-1/2}\Big/\langle S\rangle^2 , \tag{69}$$

with

$$N = \rho\pi^{3/2}\bar{\omega}_0^2\bar{z}_0 \ . \tag{70}$$

As described after Eqn. (2), N is $3\sqrt{\pi}/4$ times the mean number of molecules contained within an ellipsoid (with abrupt-boundary) with radius $\bar{\omega}_0$ and depth $\bar{z}_0 = \bar{\zeta}^{-1/2}\bar{\omega}_0$.

The dimensions of the probe volume are determined by both the focused laser and the spatial filter pinhole, but in most experimental set-ups, in order to collect as much fluorescence as possible, the pinhole size in object space is considerably larger than the focused laser beam. Eqns. (61) and (62) then simplify to

$$\alpha_{nm} \approx (n+m)/(2nm), \qquad \text{for } \sigma_C >> \sigma, \tag{71}$$

$$\beta_{nm} \approx (2^{1/n} + 2^{1/m})/2 - 1, \quad \text{for } \sigma_{Cz} >> \sigma_z . \tag{72}$$

7. IMPLEMENTATION OF FITTING BY SATURATION MODEL

The power-dependent fitting function for the ACF, which includes triplet and saturation effects, is given in Eqn. (69). The particle number, N, the triplet parameters A and $\bar{\tau}_T$, and the diffusional residence time τ_D, are the adjustable parameters to be determined by the curve fitting. The confocal parameter $\bar{\zeta}$ is a constant for the particular apparatus geometry and may be held fixed at a value determined by fitting previously collected ACF. The quantities α_{nm} and β_{nm} are also constants for a particular geometry, dependent on the laser and pinhole sizes, and could in principle be determined by curve fitting a set of previously collected ACF obtained at different powers. However, in most cases, the approximations in Eqns. (71) and (72) should suffice. $\langle S\rangle$ is the measured total count rate and $\tilde{P}$ is the measured relative laser power used during the acquisition of the ACF. From Eqn. (50), we see that the factors $\rho\chi_j$ are quantities that can be empirically determined from a polynomial fit to a measurement of the total count rate, $\langle S\rangle$, minus power-dependent background, $B(\tilde{P})$, versus relative laser power, $\tilde{P}$, for the particular apparatus and sample. (Note that when background is present, we do *not* replace N in Eqn. (69) by $N\left(1 + B/\langle S\rangle\right)^2$, as was discussed following Eqn. (2), because background is already accounted for in the factor $\langle S\rangle^2$ at the end of the equation.)

The possibility of photobleaching and other causes for distortion of the ACF, as discussed in the introduction, and in particular, detector and electronic counting saturation, especially at higher particle concentrations, as discussed in Ref. [34], will generally limit the usefulness of the saturation model to cases of moderate laser power. Therefore, we retain only the two lowest order terms of the power series expansions. Eqn. (50) gives

$$\langle S\rangle - B(\tilde{P}) \approx a_1\tilde{P} + a_2\tilde{P}^2 , \tag{73}$$

with $a_1 = \rho\chi_1$, $a_2 = \rho\chi_2$ to be determine from a quadratic fit. Eqn. (69) then gives the fitting function as

$$\begin{aligned} g_f(\tau) = N^{-1}\left(1 + A\exp(-\tau/\bar{\tau}_T)\right)\langle S\rangle^{-2}\Big\{ & a_1^2\tilde{P}^2\left[1 + \tau/\tau_D\right]^{-1}\left[1 + \bar{\zeta}\tau/\tau_D\right]^{-1/2} \\ & + 2a_2^2\tilde{P}^3\left[3/4 + \tau/\tau_D\right]^{-1}\left[2^{-1/2} + \bar{\zeta}\tau/\tau_D\right]^{-1/2}\Big\}, \qquad \text{for } \sigma_C >> \sigma,\ \sigma_{Cz} >> \sigma_z . \end{aligned} \tag{74}$$

We emphasize that the fitting function in Eqn. (74) is intended only for laser powers such that the peak irradiance at the origin, $I(0,0,0) = 2P/(\pi\omega_0^2)$, is less than ~$0.2\times I_S$. Note that if we retain only the lowest order term of Eqn. (74) and substitute $a_1 = \left(\langle S \rangle - B\right)\big/\tilde{P}$ from the lowest order term of Eqn. (73), we recover the standard model fitting function of Eqns. (2) and (3), together with the background correction factor.

8. FITTING SIMULATED ACF USING THE SATURATION MODEL

An *ab-initio* Monte Carlo simulation of FCS for cw excitation, described in Ref. [3], was used to generate sets of FCS raw data, each consisting of the times-of-arrival (TOAs) of the detected photons. The TOAs were used to numerically evaluate the ACF, by use of an algorithm similar to that described in Ref. [3]. The simulations were thus used to demonstrate the effects of triplet photophysics and saturation, and to show that curve fitting of the ACF's using Eqn. (74) can recover more consistent results for the parameter values over a limited range of excitation powers. The simulation models excitation saturation by imposing a time delay following each excitation of a molecule before the next excitation may occur, where the delay is a random real number with an exponential distribution with decay time equal to the fluorescence lifetime, or to the phosphorescence lifetime if triplet crossing occurs. We present results of simulations with apparatus parameters similar to those of the Confocor 2 [72] for two cases: (i) that of a molecule that exhibits excitation saturation (due to the finite fluorescence lifetime) with no triplet crossing, and (ii) that of a molecule that exhibits saturation effects only due to occasional triplet crossing. The fluorophore is assumed to have $\sigma_a = 2.7\times10^{-16}\text{cm}^2$ at 488 nm, with (i) τ_F = 3 ns, corresponding to I_S = 5.0 × 10^5 Wcm^{-2} and no triplet, or (ii) τ_F = 0, but τ_P = 1 μs with R =0.01, corresponding to I_S = 1.5 × 10^5 Wcm^{-2} (calculated by Eqn. (9)).

Fig. 5 presents plots of the total count rate (minus background) versus laser power at the sample for each of the cases. The plots, which are clearly non-linear due to saturation effects, are fit to the quadratic of Eqn. (73) to find the quantities (i) a_1 = 1.8×10^9 s^{-1} W^{-1}, a_2 = –7.9×10^{11} s^{-1} W^{-2}, or (ii) a_1 = 1.3×10^9 s^{-1} W^{-1}, a_2 = –1.2×10^{12} s^{-1} W^{-2}.

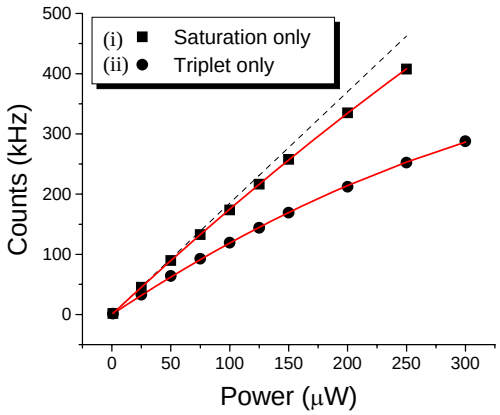

Fig. 5: Data from Monte Carlo simulations are used to form plots of the fluorescence count rate versus laser power, which exhibit nonlinearity due to saturation. The count rate plots are fit to the quadratic Eqn. (73).

The ACF's from both cases, (i) and (ii), are fit to both the standard model of Eqn. (2), with the triplet correction term from Eqn. (3) for case (ii), and to the saturation model of Eqn. (74), with A held at zero for case (i). Fig. 6 presents the graphs of only the more interesting case (ii), where triplet blinking occurs. Note that as the laser power is increased, the ACF curves develop an increasing magnitude, A, of triplet

contribution, with decay time $\bar{\tau}_T$. As discussed after Eqn. (4), the ACF becomes greater for small delays because of triplet blinking and depressed for large delays because of concomitant saturation. The inset to Fig. 6 shows that the values obtained for A and $\bar{\tau}_T$ for each curve-fitting model are approximately the same. The triplet term does not lend much flexibility in fitting the main feature of the ACF curve around $\tau \approx \tau_D$, because $\bar{\tau}_T << \tau_D$, except possibly when the triplet component is very small at low laser power. (By contrast, in Ref. [52], the added term for bleaching is such that the reciprocal of the bleaching rate obtained from the curve fit is approximately the same as τ_D.)

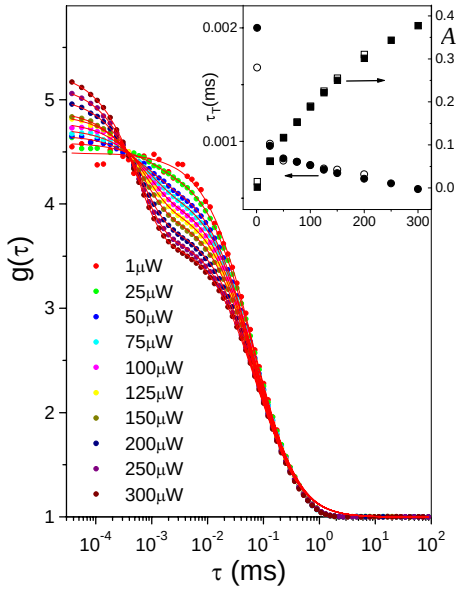

Fig. 6: The ACFs of molecules with a triplet state (from the simulated data (ii) from Fig. 5), together with curve fits to the saturation model of Eqn. (74). The ACF were also fit to the standard model. The plot in the inset shows that as the laser power is increased, A increases and $\bar{\tau}_T$ decreases, but the values obtained by fitting to the saturation model (open symbols) are essentially the same as those from the standard model (solid symbols).

A comparison of the results of the curve fitting by the standard model and the saturation model is shown in Fig. 7. Different parameter values were used in the two sets of simulations so that the data points are not overlaid.

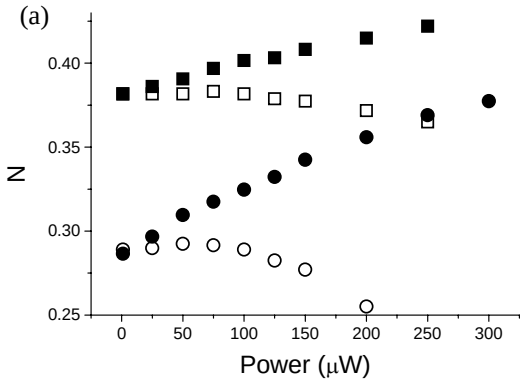

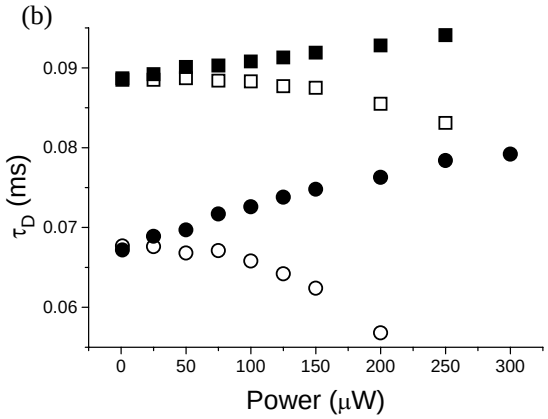

Fig. 7: The results of curve fitting to the standard model of Eqns. (2) and (3) shown as filled symbols, and to the saturation model of Eqn. (74) shown as open symbols for the cases of (i) saturation with no triplet, shown as squares, and (ii) triplet, shown as circles, as the laser power is increased. Fig. 7(a) shows N and Fig. 7(b) shows τ_D.

For the standard model (filled symbols), both the apparent particle number N and the apparent diffusional residence time τ_D are seen to increase as the laser power increases. These parameters should of course be independent of laser power. As discussed at the end of Section 2, it is not that there is an onset of systematic bias in the estimated parameters when the laser irradiance is above a particular critical 'saturation' value and that bias can be avoided by performing measurements below this point. Rather, to obtain unbiased parameters with the standard model, one needs to collect data with as low a laser power as possible. However, the data collection time increases approximately quadratically as the laser power is reduced. The increasing bias as the laser power is increased is present for both cases, i.e., for (i) saturation without no triplet kinetics, and (ii) saturation induced by triplet kinetics, but it is greater for case (ii), which has a lower value of I_S. When the ACF are fit to the saturation model (open symbols), more consistent results are obtained as the laser power is initially increased up to about 100 μW, although beyond this, the bias is then seen to be overcorrected at larger laser powers.

As might be expected, a higher order approximation of Eqn. (69) improves matters, as the successive terms in the power series expansion of Eqn. (28) have alternating signs. With simulations, where other causes of systematic errors, such as photobleaching, can be easily controlled, it is possible to extend the success of the saturation model in yielding unbiased results to higher laser powers by use of higher-order approximations, but this becomes increasingly more difficult in experiments. Instead, a more conservative approach is to use just the lowest-order saturation model (Eqn. (74)), but to develop an understanding of the limitations of the approximation, in terms of the estimated accuracy of the results, and the acceptable range of laser powers that may be used. One point to note is that when only a quadratic approximation is made to the plot of the fluorescence count rate versus laser power (Fig. 5), the values obtained for the parameters a_1 and a_2 will change slightly if the plot and fit are extended to greater powers. Different values for a_1 and a_2 will slightly alter the success of the quadratic approximation of Eqn. (74) in coping with the effects of saturation. More detailed statistical analysis would be needed to provide quantitative estimates for the final accuracy of the quadratic approximation, but as a rough guide, it may seen that the lowest-order saturation model of Eqn. (74) produces reasonably unbiased values of N and τ_D out to excitation powers that are about one-fifth of that required to yield a peak irradiance at the origin equal to the saturation intensity. Another conservative approach for data interpretation, which may be helpful in some intracellular FCS studies, is to apply both the standard and the lowest-order saturation curve-fitting models in order to estimate the upper and lower bounds to the measured values of N and τ_D.

9. USE OF THE SATURATION MODEL WITH EXPERIMENTAL ACF

In this section we discuss results from experimentally acquired ACF with curve fitting analysis using both the standard model and the saturation model of Eqn. (74). We have performed measurements with a variety of samples and labeled biomolecules and here present results for two interesting cases from solutions of (i) Alexa 488 labeled Streptavidin (Invitrogen catalog number S-32354), which has a moderate triplet component and imperfect photostability, and (ii) water soluble quantum dots (Invitrogen catalog number Q10113MP), which has excellent photostability and signal. The 488 nm line from an argon-ion laser (Spectra-Physics, 2060-10S Beamlok) was used for cw excitation of Alexa-488. The quantum dots have peak absorption at 585 nm but were excited sub-optimally using 532nm picosecond pulses from a 76MHz passively mode-locked, diode-pumped Nd:YAG laser (Spectra-Physics, Vanguard VNGD2000-76-HM532). Samples with concentrations in the nanomolar range were prepared by serial dilution using purified water (Barnstead, Nanopure D8991).

FCS measurements were performed using a custom-made apparatus based on an infinity-corrected 1.2 NA water-immersion microscope objective (Olympus, Uplanpro 60×). The objective was used with a 250 mm achromat in place of the usual 180 mm tube lens, resulting in a magnification of 83.3. A 100 micron diameter pinhole was used in all experiments and hence the spatial pinhole radius in object space was about 0.6 microns. For epi-illumination, an uncoated fused-silica substrate was used in place of the usual dichroic mirror. This was placed between the objective and tube lens and set at 45° to give ~10% Fresnel reflection of s-polarized laser light to the objective. The remaining ~90% of the laser was passed to a power meter (Coherent, LM-2VIS) to record the relative power at the sample. The laser powers reported below are 10% of the values given by the power meter and hence are approximately equal to those at the sample. As the fluorescence collected by the objective is unpolarized, about 95% is passed through the fused-silica substrate to the tube lens, pinhole, and subsequent filter. Different band pass emission filters (Omega Optical, 3rd Mellenium 500-560 nm for Alexa-488 and 617DF45 for Quantum dots) were selected based on the emission spectra of the particular sample. The filtered fluorescence was then tightly focused to the center of the active area of a SPAD single photon counting module (Perkin-Elmer, SPCM-AQR-15). The pulses from the detector were passed to the gate-input of a National Instruments PCI-6602 counter/timer data acquisition card, which was configured to record the TOA of each detected photon using an onboard 80 MHz clock. The photon TOAs were used to numerically calculate the normalized ACF using an algorithm similar to one described in Ref. [3] implemented in LabView (National Instruments). The system was used to collect ACFs from a sample of water at different laser powers, in order to measure the power-dependent background and also to characterize the detector afterpulse performance. The LabView program corrects the accumulated ACF for detector afterpulses using the method of Ref. [35]. Microcal Origin 5.0 software was used to perform unweighted least-squares curve-fitting based on a Levenberg–Marquardt algorithm. For all fits, the confocal parameter was held fixed at a value of $\overline{\zeta} = \zeta = 0.167$.

For each series of measurements, a milli-liter volume sample was placed in a cell of a chambered coverglass with coverplate (Nagle Nunc International). Control experiments were performed to check that the sample concentration did not change appreciably over the span of the experiments due to evaporation or molecular adsorption. Measurements were also made using only water to obtain calibration data for the background. The power-dependent measurements for each sample were performed in sequence of increasing power under identical conditions, with acquisition times of 10 to 100s, and repeated 3 times. The collected data were used to obtain plots of the background-subtracted count rate versus relative laser power, which were fit to quadratics to yield the quantities (i) $a_1 = 2.38\times10^8\ \mathrm{s}^{-1}\ \mathrm{W}^{-1}$, $a_2 = -3.7\times10^5\ \mathrm{s}^{-1}\ \mathrm{W}^{-1}$, for the Alexa-488 sample, and (ii) $a_1 = 5.21\times10^8\ \mathrm{s}^{-1}\ \mathrm{W}^{-1}$, $a_2 = -2.5\times10^6\ \mathrm{s}^{-1}\ \mathrm{W}^{-1}$ for the quantum dot sample.

Fig. 8 displays the average of the 3 ACFs collected from each sample for each set of laser powers, reported in microwatts, together with fits to the saturation model of Eqn. (74). For the quantum dot sample, the triplet component was held at zero for consistency of analysis, although some slope to the initial part of the ACF is apparent as the power is increased, indicating power-dependent blinking. For the Alexa-488 sample, the triplet factor is included in all fits. All curves in Fig. 8 have been rescaled by the background

correction factor $\left(1+B/\langle S\rangle\right)^{-2}$ so that the minor increase in background with increasing laser power does not contribute to power-dependent changes in the amplitudes of the plotted ACFs. For the Alexa-488 sample, the mean background and signal count rates were 120—1,000 and 4—34 × 10^3 s^{-1} with 15—200 μW of laser power and 100—10 s of data collection time for each of 3 repetitions. For the Quantum dot sample, the mean background and signal count rates were 170—850 and 1—17 × 10^3 s^{-1} with 3—300 μW of laser power and 60—10 s of data collection time for each of 3 repetitions.

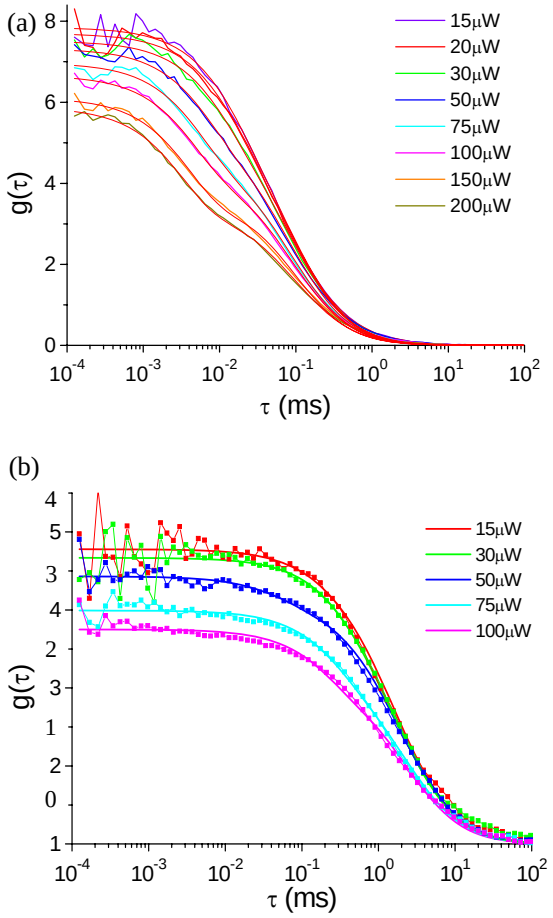

Fig. 8: Experimental ACF and fits to Eqn. (72) for different relative laser excitation powers, expressed as approximate laser power at the sample in microwatts, for (a) Alexa-488, excited by a 488 nm cw laser; and (b) Quantum dots, excited by a 532 nm 76MHz picosecond pulses.

The results of the fits by the standard model of Eqns. (2) and (3) and the saturation model of Eqn. (74) are compared in Fig. 9. For the standard model, the apparent particle number N and diffusional residence time τ_D each increase as the laser power increases. For the saturation model, the parameters retain more consistent values, at least for laser powers below ~100 μW. It should be emphasized that it is not necessary to collect a series of ACFs over a range of laser powers in order to implement the saturation model. All that is needed is a measurement of the total count rate versus laser power from the sample, a similar measurement from water to account for background, and a single measurement of an ACF at a measured laser power. The purpose of presenting a series of ACF here is to illustrate that the lowest-order saturation model yields approximately consistent parameter values over a range of laser powers typically used in FCS.

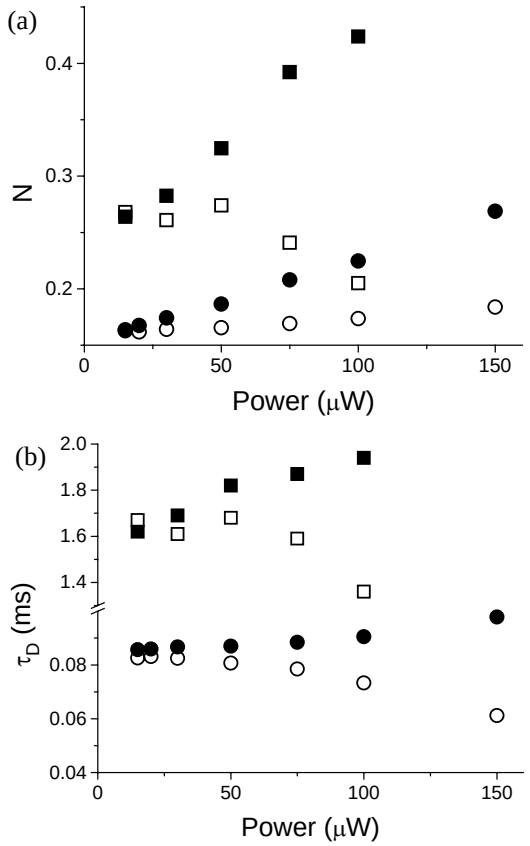

Fig. 9: The results of curve fitting to the standard model of Eqns. (2) and (3) shown as filled symbols, and to the saturation model of Eqn. (74) shown as open symbols for the experiments of (i) Alexa-488 (from Fig. 8 (a)), shown as circles; and (ii) quantum dots (from Fig. 8 (b)), shown as squares (with $A = 0$, i.e., no triplet component). Fig. 9(a) shows N and Fig. 9(b) shows τ_D.

10. CONCLUSIONS

Practitioners of quantitative FCS face a difficult task in managing a range of possible systematic errors. In many cases, excitation saturation presents the primary cause for systematic errors and it results in bias in the particle number N and diffusional residence time τ_D found from curve fitting the ACF with the standard model. Saturation typically arises from the finite fluorescence lifetime, which delays the repopulation of the ground state following excitation, and it is accentuated by transitions to long-lived dark states, such as the triplet state. Such transitions are usually accounted for by adding an exponential term, with microsecond-range decay time, in the fitting function of the ACF (Eqn. (3)), to account for fast blinking of molecules, but when such fast kinetics are evident, saturation effects are also present. Studies in the literature, Monte Carlo simulations presented in Section 8 and Fig. 6, and experimental results presented in Section 9 and Figs. 8, all show that the amplitude of the ACF decreases, and the decay time increases, with increase in laser power (even when background remains negligible). It is not that these changes occur only when the laser power is above a critical value, but rather, the power dependence of the ACF occurs even at infinitesimal laser powers. It is usually not practical to perform FCS at the lowest possible laser power, because the collection time increases approximately quadratically with decrease in count rate, and moreover, corrections for background become approximately quadratically greater as the signal to background decreases. The standard model used for fitting the ACF (Eqns. (1) and (2)) does not contain any dependence on the laser power, but experiments clearly show that the ACF is power dependent.

The power dependence of the ACF is due primarily to saturation and triplet effects. This paper includes a rate equation theory of molecular photophysics, including saturation and triplet kinetics, for cases of sub-nanosecond pulsed, sub-picosecond pulsed, or continuous wave excitation, by either one- or two-photon

mechanisms. This theory is used to show that the ideal 3-D Gaussian profile of fluorescence is distorted because of saturation, but for parameters of interest, the distorted profile can be expressed as a weighted sum of 3D-Gaussians of calculable widths (Eqn. (46)), with power-dependent weights that can be determined by measuring the total fluorescence count rate versus power (Eqn. (50)). A derivation of the ACF, formulated in terms of single-photon detection from single molecules diffusing through the distorted profile (rather than intensity fluctuations from concentration fluctuations), leads to a new model for the ACF fitting function that is explicitly power-dependent (Eqn. (69)). The lowest order term of this equation is the same as the standard model. The two terms of lowest order in the relative laser power provide a useful lowest-order power-dependent saturation model for the ACF (Eqn. (72)), for situations in which triplet and saturation effects are still small, i.e., for peak irradiance below ~0.2 times the saturation irradiance I_S. The new saturation model contains no additional fitting parameters, but it does require a separate calibration measurement of the total fluorescence count rate versus relative laser power and knowledge of the relative laser power at which the FCS measurement was acquired.

Ab initio Monte Carlo simulations and experiments with continuous and pulsed laser excitation, using Alexa-488 and quantum dots, are used to show that the lowest-order saturation model provides more consistent estimates of the particle number N and diffusional residence time τ_D over a range of laser powers typically used in FCS (about 0 — 200 μW) whereas the standard model produces unbiased estimates only as the power tends to zero. A quick calibration measurement of the count rate versus relative laser power used with the saturation model for FCS should provide a useful method for determining upper and lower bounds to measured parameter values in situations where data collection times are limited. Saturation effects will also be important in the quantitative interpretation of 2-state FCS measurements, particularly where the brightness values of the two states differ.

ACKNOWLEDGEMENTS

We acknowledge financial and equipment loan support for this work from LI-COR, Inc., Lincoln, NE; Abbott Laboratories*, Chicago, IL; Perkin Elmer, Vaudreuil, Canada; the National Science Foundation; National Institutes of Health grant R03EB004586; and the State of Tennessee Center of Excellence in Laser Applications**. We thank Kerry Swift*, Edmund Matayoshi*, and David Ball** for discussions and assistance in projects leading up to this paper.

REFERENCES:

[1] Rigler, R. and Elson, E.S. (2001) Eds. *Fluorescence Correlation Spectroscopy: Theory and Applications*, Springer, Berlin.
[2] Widengren, J. and Mets, U. (2002) in *Single-Molecule Detection in Solution–Methods and Applications*, (Zander, C.; Enderlein, J. and Keller, R.A. Eds.), Wiley-VCH, Berlin, pp. 69-95.
[3] Davis, L.M.; Williams, P.E.; Ball, D.A.; Matayoshi, E.D. and Swift, K.M. (2003) *Curr. Pharm. Biotech.* **4**, 451-462.
[4] de Jong, L.A.A.; Uges, D.R.A.; Franke, J.P. and Bischoff, R. (2005) *J. Chromatogr. B*, **829** (1-2), 1-25.
[5] Hong, H. and Granick, S. (2005) *J. Polym. Sci. Part B: Polym. Phys.*, **43**(23): 3497-3502.
[6] Chattopadhyay, K.; Elson, E.L. and Frieden, C. (2005) *Proc. Natl. Acad. Sci. USA.*, **102**(7): 2385-2389.
[7] Banks, D.S. and Fradin, C. (2005) *Biophys. J.*, **89**(5), 2960-2971.
[8] Bacia, K.; Kim, S.A. and Schwille, P. (2006) *Nature Methods*, **3**(2), 83-89.
[9] Donsmark, J.; Jorgensen, L.; Mollmann, S.; Frokjaer, S. and Rischel, C. (2006) *Pharm. Res.*, **23**(1), 148-155.
[10] Schwille, P.; Korlach, J. and Webb, W.W. (1999) *Cytometry*, **36**(3), 176-182.
[11] Birkmann, E.; Schafer, O.; Weinmann, N.; Dumpitak, C.; Beekes, M.; Jackman, R.; Thorne, L. and Riesner, D. (2006) *Biol. Chem.*, **387**(1), 95-102.
[12] Rieger, R.; Rocker, C. and Nienhaus, G.U. (2005) *Am. J. Phys.*, **73**(12), 1129-1134.
[13] Berglund, A.J. and Mabuchi, H., (2005) *Opt. Exp.*, **13**(20): 8069-8082.
[14] Saxton, M.J. (2005) *Biophys. J.*, **89**, 3678-3679.
[15] Masuda, A.; Ushida, K. and Riken, T.O. (2005) *Biophys. J.*, **89**(5), 3584-3591.
[16] Wawrezinieck, L.; Rigneault, H.; Marguet, D. and Lenne, P.F. (2005) *Biophys. J.*, **89**, 4029-4042.

[17] Masuda, A.; Ushida, K. and Okamoto, T. (2005) *Phys. Rev. E*, **72**(6), Art. No. 060101.
[18] Webb, W.W. (2001) *Appl. Opt.*, **40**, 3969-3983.
[19] Elson, E.L. (2004) *J. Biomed. Opt*., **9**(5), 857-864.
[20] Thompson, N.L. (2002) *Curr. Opin. Struc. Biol*., **12**, 634-641.
[21] Schwille, P. (2001) *Cell Biochem. Biophys*., **34**(3), 384-408.
[22] Hess, S.T.; Huang, S.H.; Heikal, A.A. and Webb, W.W. (2002) *Biochem.*, **41**(3), 697-705.
[23] Magde, D.; Elson, E.L. and Webb, W.W. (1972) *Phys. Rev. Lett.*, **29**, 705-708.
[24] Elson, E.L. and Magde, D. (1974) *Biopolymers*, **13**, 1-27.
[25] Magde, D.; Webb, W.W. and Elson, E.L. (1974) *Biopolymers*, **13**, 29-61.
[26] Ehrenberg, M. and Rigler, R. (1974) *Chem. Phys.*, **4**, 390-401.
[27] Berne, B.J. and Pecora, R. (1976) in *Dynamic light scattering*, Wiley, New York; (esp. Sec. 6.6).
[28] Shera, B.E.; Seitzinger, N.K.; Davis, L.M.; Keller, R.A. and Soper, S.A. (1990) *Chem. Phys. Lett.* **174**(6), 553-557.
[29] Qian, H. and Elson, E.L. (1991) *Appl. Opt*. **30,** 1185-1195.
[30] Rigler, R.; Mets, U.; Widengren, J. and Kask, P. (1993) *Eur. Biophys. J. Biophys. Lett.*, **22**(3), 169-175.
[31] Li, L.Q. and Davis, L.M. (1993) *Rev. Sci. Instrum.*, **64**, 1524-1529.
[32] Spinelli, A.; Davis, L.M. and Dautet, H. (1996) *Rev. Sci. Instrum.*, **67**, 55-61.
[33] Enderlein, J.; Gregor, I.; Patra, D. and Fitter, J. (2004) *Curr. Pharm. Biotech.*, **5**(2), 155-161.
[34] Nishimura, G. and Kinjo, M. (2005) *Appl. Opt*., **44**, 3458-3467.
[35] Zhao, M.; Jin, L.; Chen, B.; Ding, Y.; Ma, H. and Chen, D.Y. (2003) *Appl. Opt*., **42**(19), 4031-4036.
[36] Enderlein, J. and Gregor, I. (2005) *Rev. Sci. Instrum.*, **76**, 033102-1-033102-5 (2005)
[37] Schatzel, K.; Drewel, M. and Stimac, S. (1988) *J. Mod. Opt.*, **35**, 711-718.
[38] Saffarian, S. and Elson, E.L. (2003) *Biophys. J*., **84**, 2030-2042.
[39] Davis, L.M.; Ball, D.A.; Williams, P.E.; Matayoshi, E.D. and Swift, K.M. (2003) in *Microarrays and Combinatorial Technologies for Biomedical Applications*, (Nicolau, D.V. and Raghavachari, R. Eds.), Proc. SPIE, **4966**, pp. 117-128.
[40] Hess, S.T. and Webb, W.W. (2002) *Biophys. J*., **83**, 2300-2317.
[41] Aragón, S.R. and Pecora, R. (1976) *J. Chem. Phys*., **64**, 1791-1803.
[42] Edman, L. (2000) *J. Phys. Chem. A*, **104**, 6165-6170.
[43] Koppel, D.E. (1974) *Phys. Rev. A*, **10**, 1938-1945.
[44] Bunfield, D.H. and Davis, L.M. (1998) *Appl. Opt*., **37**, 2315-2326.
[45] Wohland, T.; Rigler, R. and Vogel, H. (2001) *Biophys. J.*, **80**, 2987-2999.
[46] Nishimura, G. and Kinjo, M. (2004) *Anal. Chem*., **76**, 1963-1970.
[47] Ding, J.Y.; Chen, B.; Meng, F.B. and Ma, H. (2004) *Acta Physica Sinica*, **53**, 2503-2508 (In Chinese).
[48] Davis, L.M.; Shen, G.Q. and Ball, D.A. (2005) in *Multiphoton Microscopy in the Biomedical Sciences V*, (A. Periasamy, P.T.C. So, Eds.), Proc. SPIE, **5700**, pp 128-137.
[49] Mertz, J. (1998) *Eur. Phys. J. D*, **3**, 53-66.
[50] Marrocco, M. (2004) *Appl. Opt*. **43**, 5251-5262.
[51] Cianci, G.C.; Wu, J.R. and Berland, K.M. (2004) *Microsc. Res. Tech.*, **26**, 473-488.
[52] Nagy, A.; Wu, J.R. and Berland, K.M. (2005) *Biophys. J*., **89**, 2077-2090.
[53] Nagy, A.; Wu, J.R. and Berland, K.M. (2005) *J. Biomed. Opt*., **10**, Art. No. 044015.
[54] Niesner, R.; Roth, W. and Gericke, K.H. (2004) *ChemPhysChem*, **5**, 678-687.
[55] Gregor, I.; Patra, D. and Enderlein, J. (2005) *ChemPhysChem*, **6**, 164-170.
[56] Enderlein, J.; Gregor, I.; Patra, D.; Dertinger, T. and Kaupp, U.B. (2005) *ChemPhysChem*, **6**, 2324-2336.
[57] Weisshart, K.; Jungel, V. and Briddon, S.J. (2004) *Curr. Pharm. Biotech*., **5**, 135-154.
[58] Krouglova, T.; Vercammen, J. and Engelborghs, Y. (2004) *Biophys. J*., **87**, 2635-2646.
[59] Eggeling, C.; Jager, S.; Winkler, D. and Kask, P. (2005) *Curr. Pharm. Biotech*., **6**, 351-371.
[60] Widengren, J. and Seidel, C.A.M. (2000) *Phys. Chem. Chem. Phys*., **2**, 3435-3441.
[61] Huang, Z.; Ji, D.; Wang, S.; Xia, A.; Koberling, F.; Patting, M. and Erdmann, R. (2006) *J. Phys. Chem. A*, **110**, 45-50.
[62] Widengren, J.; Rigler, R. and Mets, U. (1994) *J. Fluorescence*, **4**, 255-258.
[63] Widengren, J.; Mets, U. and Rigler, R. (1995) *J. Phys. Chem*. **99**, 13368-13379.

[64] Berland, K. and Shen, G.Q. (2003) in *Multiphoton Microscopy in the Biomedical Sciences III*, (A. Perisamy, and P.T.C. So, Eds.), Proc. SPIE, **4963**, pp. 1-12 (2003).
[65] Berland, K. and Shen, G.Q. (2003) *Appl. Opt.* **42**, 5566-5576.
[66] Osborne, M.A.; Balasubramanian, S.; Furey, W.S. and Klenerman, D. (1998) *J. Phys. Chem. B* **102**, 3160-3167.
[67] Boyd, R.W. (1991) in *Nonlinear Optics*, Academic Press, San Diego.
[68] Lakowicz, J.R. (1999) in *Principles of Fluorescence Spectroscopy*, Kluwer Academic / Plenum Publishers, New York.
[69] London, R. (2000) in *The Quantum Theory of Light*, (Third Edition) Oxford University Press, New York; esp. pp. 79-81.
[70] W.T. Silvast (1996) *Laser Fundamentals*, Cambridge University Press, Melbourne.
[71] Pastirk, I.; Dela Cruz, J.M.; Walowicz, K.A.; Lozovoy, V.V. and Dantus, M. (2003) *Opt. Express* **11**, 1695-1701.
[72] Jankowski, T. and Janka, R. (2001) pp. 331-359 in Ref. [1].